


# A first-principles study on remote van der Waals epitaxy through a graphene monolayer on semiconductor substrates

Rui Hou(侯锐) and Shenyuan Yang(杨身园)

**Citation:**Chin. Phys. B, 2023, 32 (**6**): 066801. DOI: 10.1088/1674-1056/ac92d6
Journal homepage: http://cpb.iphy.ac.cn; http://iopscience.iop.org/cpb

**What follows is a list of articles you may be interested in**

---

## Visualizing interface states in $In_2Se_3$–$WSe_2$ monolayer lateral heterostructures

Da Huo(霍达), Yusong Bai(白玉松), Xiaoyu Lin(林笑宇), Jinghao Deng(邓京昊), Zemin Pan(潘泽敏), Chao Zhu(朱超), Chuansheng Liu(刘传胜), and Chendong Zhang(张晨栋)
Chin. Phys. B, 2023, 32 (**5**): 056803. DOI: 10.1088/1674-1056/acbaef

## Atomistic insights into early stage corrosion of bcc Fe surfaces in oxygen dissolved liquid lead-bismuth eutectic (LBE-O)

Ting Zhou(周婷), Xing Gao(高星), Zhiwei Ma(马志伟), Hailong Chang(常海龙), Tielong Shen(申铁龙), Minghuan Cui(崔明焕), and Zhiguang Wang(王志光)
Chin. Phys. B, 2023, 32 (**3**): 036801. DOI: 10.1088/1674-1056/ac834b

## Evolution of microstructure, stress and dislocation of AlN thick film on nanopatterned sapphire substrates by hydride vapor phase epitaxy

Chuang Wang(王闯), Xiao-Dong Gao(高晓冬), Di-Di Li(李迪迪), Jing-Jing Chen(陈晶晶), Jia-Fan Chen(陈家凡), Xiao-Ming Dong(董晓鸣), Xiaodan Wang(王晓丹), Jun Huang(黄俊), Xiong-Hui Zeng(曾雄辉), and Ke Xu(徐科)
Chin. Phys. B, 2023, 32 (**2**): 026802. DOI: 10.1088/1674-1056/ac6865

## Molecular beam epitaxy growth of quantum devices

Ke He(何珂)
Chin. Phys. B, 2022, 31 (**12**): 126804. DOI: 10.1088/1674-1056/aca6d3

## Gate tunable Rashba spin-orbit coupling at $CaZrO_3$/$SrTiO_3$ heterointerface

Wei-Min Jiang(姜伟民), Qiang Zhao(赵强), Jing-Zhuo Ling(凌靖卓), Ting-Na Shao(邵婷娜), Zi-Tao Zhang(张子涛), Ming-Rui Liu(刘明睿), Chun-Li Yao(姚春丽), Yu-Jie Qiao(乔宇杰), Mei-Hui Chen(陈美慧), Xing-Yu Chen(陈星宇), Rui-Fen Dou(窦瑞芬), Chang-Min Xiong(熊昌民), and Jia-Cai Nie(聂家财)
Chin. Phys. B, 2022, 31 (**6**): 066801. DOI: 10.1088/1674-1056/ac5396

---

# A first-principles study on remote van der Waals epitaxy through a graphene monolayer on semiconductor substrates

Rui Hou(侯锐)[1,2] and Shenyuan Yang(杨身园)[1,2,†]

[1] *State Key Laboratory of Superlattices and Microstructures, Institute of Semiconductors, Chinese Academy of Sciences, Beijing* 100083, *China*
[2] *College of Materials Science and Opto-electronic Technology, University of Chinese Academy of Sciences, Beijing* 100049, *China*

(Received 15 August 2022; revised manuscript received 15 August 2022; accepted manuscript online 19 September 2022)

To investigate the mechanism of remote epitaxy, where the overlayer can follow the same crystalline structure as the underlying semiconductor substrate through a thin two-dimensional interlayer, we systematically study the potential fluctuations of graphene covered Si, GaAs, and GaN substrates from first-principles. We find that the uneven semiconductor surface, the distorted graphene, and the non-uniform interface charge transfer make significant contributions to the potential fluctuation. The semiconductor substrate with different surface reconstructions and orientations will generate different potential fluctuations through the graphene interlayer. We also calculate and compare the adsorption of adatoms on graphene covered substrates. The adsorption energies of adatoms not only depend on their distances to the underlying semiconductor surface, but are also sensitive to the direction of the charge transfer at the graphene/substrate interface. Changing the semiconductor reconstruction or orientation could even reverse the order of the adsorption energies of cation and anion adatoms by reversing the interface charge transfer direction, leading to a change in the growth orientation of the overlayer. Our study improves the understanding of the mechanism of remote epitaxy, and reveals that it is possible to control the initial nucleation and orientation of overlayers by changing the semiconductor reconstructions and/or orientations in remote epitaxy.

**Keywords:** interface, adsorption, remote epitaxy, first-principles

**PACS:** 68.35.–p, 68.43.Bc, 73.90.+f, 71.15.Mb **DOI:** 10.1088/1674-1056/ac92d6

## 1. Introduction

Epitaxy growth has been widely used to produce high-quality single-crystalline films or nanostructures required for high-performance electronic and optoelectronic devices.[1–3] In conventional epitaxy, strong covalent bonds are formed at the interface between the substrate and the overlayer.[4,5] The lattice mismatch in a heteroepitaxy system inevitably induces crystalline defects such as dislocations in the overlayer above a critical thickness, severely degrading the performance of the devices.[6–8] Several methods have been developed to address this problem in highly lattice-mismatched heteroepitaxy systems. However, pseudomorphic growth can avoid the formation of dislocations only in thin films.[9–11] Introducing buffer layers or surfactants can lower the density of dislocations but requires complicated processes.[6–8,12]

In recent years, van der Waals (vdW) epitaxy has attracted considerable interest as a promising method to grow high-quality three-dimensional (3D) materials by introducing two-dimensional (2D) materials as an interlayer.[13–15] Due to the absence of dangling bonds on the 2D material surface and the weak vdW interaction at the interface, the requirement of lattice match can be greatly released in vdW epitaxy.[13,15] Various thin films with large lattice mismatch have been successfully synthesized on 2D coated substrates.[15–19] Recently, Kim *et al.* reported that the overlayer could follow the crystalline structure of the underlying substrate since the 2D interlayer is transparent to the remote interactions between the substrate and the overlayer,[20] which is referred to as remote epitaxy.[20,21] Remote epitaxy has been applied to the growth of single crystalline GaAs,[20,21] nitrides,[22–26] ZnO,[27–29] and other 3D materials.[30–33] These films show good quality with small interface stress and low dislocation densities compared to those synthesized by conventional heteroepitaxy.[20,24] Moreover, the overlayer can be exfoliated from the substrate, which is suitable for flexible device fabrication.[34,35] The fabricated devices exhibited comparable or even better performance than their conventional counterparts.[20,25,26] Therefore, remote epitaxy via a 2D interlayer allows the growth of high-quality, strain-free, and flexible single crystalline films on various substrates.

However, the mechanism of remote epitaxy has not been fully understood. Kong *et al.* explained remote epitaxy as the transparency of the 2D interlayer to the potential generated by the underlying substrates.[21] The potential fluctuations penetrating through the thin 2D interlayer can determine the favorable adsorption sites of the coming adatoms, the nucleation, and the growth of the overlayer. Kong *et al.* demonstrated that remote epitaxy can be governed by the polarities of the 2D interlayer and the substrate. Substrates with stronger polarities can generate a larger potential fluctuation through the 2D interlayer.[21] On the other hand, Jeong *et al.* attributed re-

†Corresponding author. E-mail: syyang@semi.ac.cn
© 2023 Chinese Physical Society and IOP Publishing Ltd 

mote epitaxy to the interface charge transfer and the interface dipole.[27,28] The interface charge transfer induces an interface dipole and electric field, which can penetrate the thin 2D interlayer and attract adatoms. By combining experiments and calculations, they showed that stronger interface interactions induced stronger interface charge transfer, and thus the interface dipole could penetrate through thicker graphene layers.[27,28] However, the relationship between the potential fluctuation and the interface charge transfer is unclear. The effects of substrate reconstructions have not been considered in previous studies. Moreover, the adsorption of adatoms at the initial nucleation stage has not been systematically studied in detail.[21]

In this work, we systematically investigate the remote epitaxy of different semiconductor substrates (subs) covered by a graphene (Gr) monolayer. We choose Si, GaAs, and GaN with different polarities as substrates, and consider different surface reconstructions and/or different orientations. We find that the potential fluctuation of the Gr/sub compound substrates highly depends on the structures of the semiconductor surface and graphene. Flat substrate surfaces and a graphene monolayer generate relatively small potential fluctuation. Rough surfaces generate large potential fluctuation. If the graphene monolayer is distorted due to the interface interaction, it will also make a remarkable contribution to the potential fluctuation. In addition, the nonuniform interface charge transfer will locally modify the potential distribution, further changing the potential fluctuation. We also study the adsorption of adatoms on Gr/sub compound substrates. The adsorption energies of adatoms highly depend on the charge transfer at the Gr/sub interface. Changing the reconstruction and orientation of the semiconductor substrates can change the adsorption energies of cations and anions, or even reverse the sequence of the adsorption energies. This will change the nucleation and the growth orientation of the overlayer. Our studies provide a better understanding of the mechanism of remote epitaxy, and demonstrate that it is possible to control the nucleation and orientation of overlayers by changing the semiconductor substrates in remote epitaxy.

## 2. Computational methods

Our first-principles calculations based on density functional theory are performed using the Vienna *ab initio* simulation package (VASP).[36] We adopt the projector-augmented wave potential (PAW)[37] and the generalized-gradient approximation of Perdew–Burke–Ernzerhof (PBE)[38] for the exchange–correlation functional. The energy cutoff of the plane wave basis set is 400 eV. All surfaces are modeled using thick slabs of six (for GaAs and GaN) or eight (for Si) bilayers with the bottom passivated by pseudohydrogen atoms. To minimize the in-plane strain in graphene, the Si(001) $2\times2$, GaAs(001) $4\times2$, and GaN($10\bar{1}0$) $2\times4$ surface cells are chosen to match the $3\times2$, $6\times2$, and $4\times3$ rectangular unit cells of graphene, respectively, while the $3\times3$ surface cells of both GaN($000\bar{1}$) and GaN(0001) are matched to the $4\times4$ unit cell of graphene. A vacuum layer larger than 15 Å thick is introduced along the surface normal direction ($z$ direction) to avoid unphysical interactions between images. The first Brillouin zone is sampled with a $12\times12\times12$ Monkhorst–Pack[39] grid for bulk semiconductors. A similar $k$-point density in the $xy$ plane is used for the surface and interface calculations. All the systems are fully relaxed until the Hellmann–Feynman forces on each atom are less than 0.01 eV/Å. The DFT-D3 method is adopted to calculate the vdW interactions.[40] Dipole correction along the $z$ direction is also considered in this work. The calculated lattice constants for zinc-blende Si and GaAs are 5.41 Å and 5.63 Å, respectively. The lattice constants for wurtzite GaN are $a=3.21$ Å and $b=5.24$ Å. All the structure parameters are in good agreement with previous theoretical and experimental results.[41–44]

## 3. Results and discussion

### 3.1. Gr/Si(001) compound substrates

First, we study the remote epitaxy of the graphene covered Si(001) surface as a prototype of non-polar substrates. We consider the Si(001)-$(1\times1)$ truncated surface and $(2\times1)$ reconstructed surface to investigate the effects of surface reconstructions. The optimized configurations of the two Gr/Si(001) interfaces are shown in Figs. 1(a) and 1(b). The Si(001)-$(1\times1)$ truncated surface is unstable, since each surface Si dangling bond is unsaturated and reactive. The distance between graphene and the surface Si atoms is 3.55 Å, in good agreement with previous calculations of 3.5 Å.[21] The Si(001)-$(2\times1)$ reconstructed surface is one of the stable reconstructions due to the formation of asymmetric Si–Si dimers.[45] On the $(2\times1)$ reconstructed surface, the distances from graphene to the higher and lower surface Si atoms are 3.38 Å and 3.99 Å, respectively. The large interface distances indicate weak vdW interactions between graphene and the Si(001) surface, regardless of the surface reconstructions. We compare the interface interactions per area of the two systems, which are calculated using

$$E_{\text{interf}}=(E_{\text{Gr/sub}}-E_{\text{sub}}-E_{\text{Gr}})/A. \tag{1}$$

Here, $E_{\text{Gr/sub}}$, $E_{\text{sub}}$, and $E_{\text{Gr}}$ are the energies of the Gr/sub compound substrate, the isolated semiconductor substrate, and the isolated graphene monolayer, respectively, and $A$ is the inplane area of the supercell. The interface interactions are calculated to be $-14.28$ meV/Å$^2$ and $-11.26$ meV/Å$^2$ for Gr/Si(001)-$(1\times1)$ and Gr/Si(001)-$(2\times1)$, respectively. Clearly, the unstable $(1\times1)$ truncated surface has a stronger

interaction with graphene than the stable $(2 \times 1)$ reconstructed surface.

To further analyze the interface interaction, we plot the difference charge densities of the two Gr/Si(001) interfaces in Fig. 1(b). The difference charge density $\Delta\rho$ is defined as

$$\Delta\rho = \rho_{\mathrm{Gr/sub}} - \rho_{\mathrm{sub}} - \rho_{\mathrm{Gr}}, \tag{2}$$

where $\rho_{\mathrm{Gr/sub}}$, $\rho_{\mathrm{sub}}$, and $\rho_{\mathrm{Gr}}$ are the charge densities of the Gr/sub compound substrate, the semiconductor substrate, and the graphene monolayer in frozen coordinates, respectively. The yellow and cyan colors denote electron accumulation and depletion, respectively. We can clearly see that electrons transfer from graphene to the Si(001) surface at both interfaces. On the $(1 \times 1)$ truncated surface, each surface Si atom gains electrons from graphene. The charge depletion on graphene is almost uniform around 0.003 $e$/atom–0.006 $e$/atom from Bader analysis.[46] On the $(2 \times 1)$ reconstructed surface, the charge redistribution is mainly localized near the higher surface Si atoms, with a maximum electron depletion of 0.002 $e$/atom on graphene. The weaker charge transfer is consistent with the weaker interface interaction in Gr/Si(001)-$(2 \times 1)$ than Gr/Si(001)-$(1 \times 1)$, as discussed above.

In previous studies, Kong *et al.* explained remote epitaxy as a result of the electrostatic potential fluctuations from the substrate penetrating through graphene,[21] whereas Jeong *et al.* argued that the Gr/sub interface charge transfer and the induced interface dipole generate a strong potential field through graphene, leading to remote epitaxy.[27,28] Here, we find that a stronger interface charge transfer does not always generate a larger potential fluctuation. Figure 1(c) shows the potential fluctuations on a plane 3 Å above the graphene monolayer for the two systems. Although the interface interaction of Gr/Si(001)-$(1 \times 1)$ is stronger, the potential fluctuation is only 19.25 meV. In contrast, Gr/Si(001)-$(2 \times 1)$ has a larger potential fluctuation of 39.85 meV. The potential of the Gr/Si compound substrate can be decomposed into three contributions: the isolated graphene, the isolated Si substrate, and the interface charge redistribution. The former two contributions can be readily calculated from frozen coordinates. In Gr/Si(001)-$(1 \times 1)$, the isolated flat graphene monolayer and the isolated smooth surface generate potentials with small fluctuations of 13.77 meV and 10.49 meV (Fig. S1 in the supplementary information), respectively. The sum of the potentials of isolated graphene and isolated substrate (denoted as Gr + Si) is also uniform, with a fluctuation of 19.33 meV. Besides, the uniform interface charge transfer can be considered as a dipole layer, which induces a uniform shift of the potential, and thus has little effect on the potential fluctuation. As a result, the distribution of the potential sum is almost the same as that of the compound substrate (red and blue lines in Fig. 1(d)). Therefore, the potential fluctuation on Gr/Si(001)-$(1 \times 1)$ mainly originates from the Si(001)-$(1 \times 1)$ surface and the graphene monolayer.

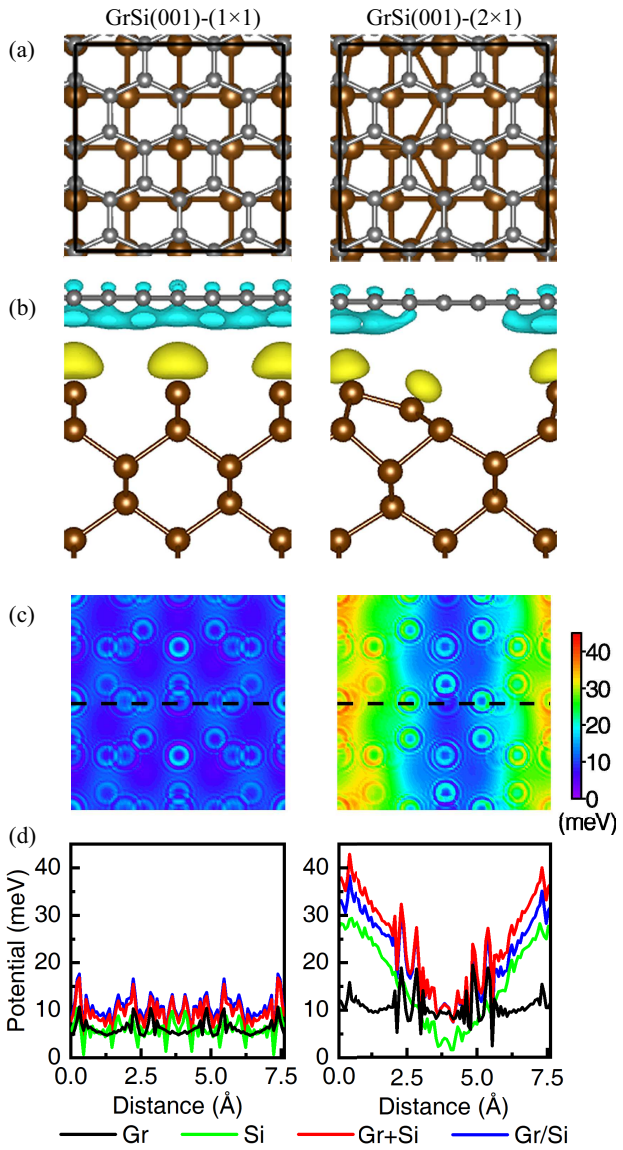



**Fig. 1.** (a) Top views of the Gr/Si(001)-$(1 \times 1)$ and Gr/Si(001)-$(2 \times 1)$ interfaces. The brown and gray balls represent Si and C atoms, respectively. (b) Difference charge densities of the two interfaces. The isosurface value is 0.0005 $e$/Bohr$^3$. (c) Potential fluctuation maps of the two interfaces. (d) Potential fluctuations of the isolated graphene Gr, isolated substrate Si, potential sum Gr + Si, and compound substrate Gr/Si along the black dashed lines in (c).

In Gr/Si(001)-$(2 \times 1)$, the uneven Si(001)-$(2 \times 1)$ reconstructed surface generates a non-uniform potential with a large fluctuation of 31.87 meV (Fig. S1 in the supplementary information), where the potential above the high Si atom is much higher than that between the dimer rows (Fig. 1(d)). The potential fluctuation of the isolated graphene is 19.76 meV, and the potential sum Gr + Si has a fluctuation of 44.43 meV. However, the potential fluctuation of the Gr/Si(001)-$(2 \times 1)$ compound substrate is slightly smaller (39.85 meV). The difference can be attributed to the non-uniform interface charge transfer. As discussed before, the interface charge transfer is mainly localized above the higher surface Si atoms in

Gr/Si(001)-(2 × 1). The non-uniform electron transfer from graphene to the substrate induces a localized upward interface dipole, locally decreasing the potential above the higher Si atoms, as seen from the difference between the red and blue lines above the higher Si atoms in Fig. 1(d). Therefore, the potential fluctuation of the Gr/Si(001)-(2 × 1) compound substrate is slightly smaller than the potential sum Gr + Si. This example demonstrates that the non-uniform interface charge transfer could also contribute to the potential fluctuation.

### 3.2. Gr/GaAs(001) compound substrates

We next study the polar GaAs(001) substrates covered by a graphene monolayer. We consider the As-terminated GaAs(001)-(1 × 1) truncated surface, $\beta(2\times4)$, and $\beta2(2\times4)$ reconstructed surfaces. The (1 × 1) truncated surface is smooth but unstable with unsaturated dangling bonds. As shown in the left panel of Figs. 2(a) and 2(b), the graphene monolayer is flat with a distance of 3.55 Å to the surface. The interface interaction is −15.35 meV/Å$^2$. The isolated graphene and GaAs surface generate uniform potentials with small fluctuations of 13.86 meV and 8.98 meV, respectively (Fig. S2 in the supplementary information). As shown in Fig. 2(b), the charge transfer from graphene to the truncated surface is uniform, with a charge depletion of 0.001 *e*/atom on graphene. The uniform interface charger transfer has little effect on the potential fluctuation. Therefore, the potential fluctuation of the Gr/GaAs(001)-(1 × 1) compound substrate is 19.31 meV (Fig. 2(c)), very close to the potential sum Gr + GaAs, as shown in Fig. 2(d).

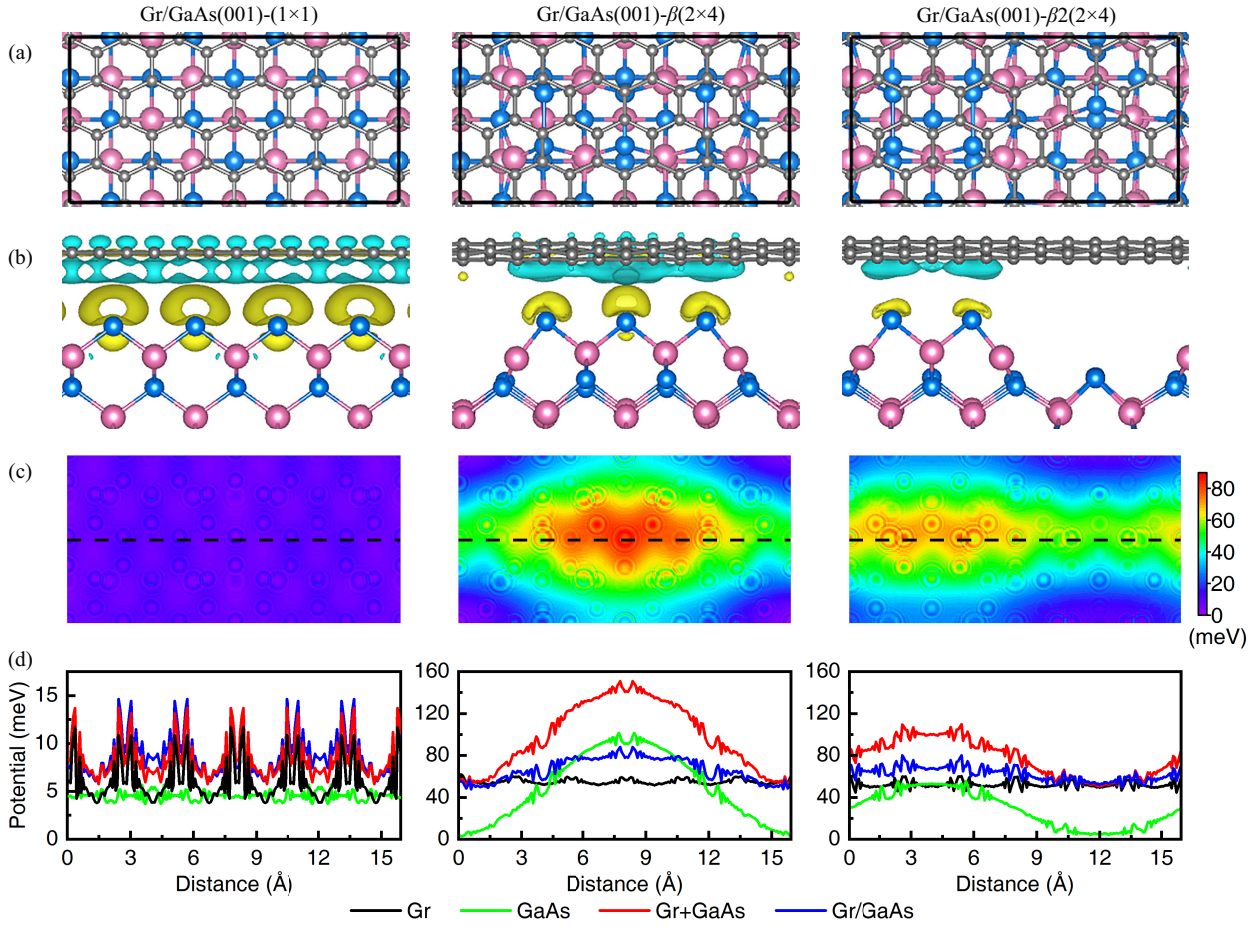



**Fig. 2.** (a) Top views of the Gr/GaAs(001)-(1 × 1), Gr/GaAs(001)-$\beta(2\times4)$, and Gr/GaAs(001)-$\beta2(2\times4)$ interfaces. The pink, light blue, and gray balls represent Ga, As, and C atoms, respectively. (b) Difference charge densities of the three interfaces. The isosurface value is 0.0002 *e*/Bohr$^3$. (c) Potential fluctuation maps of the three interfaces. (d) Potential fluctuations of the isolated graphene Gr, isolated substrate GaAs, potential sum Gr + GaAs, and compound substrate Gr/GaAs along the black dashed lines in panel (c).

GaAs(001)-$\beta(2\times4)$ and $\beta2(2\times4)$ are stable reconstructions with three and two As–As surface dimers per (2 × 4) surface cell, respectively.[47,48] As shown in Fig. 2(b), the graphene layers on the two reconstructed surfaces are distorted due to the uneven surface morphology. The average heights from graphene to the surfaces are around 3.4 Å, with weak interface interactions of −15.00 meV/Å$^2$ and −12.33 meV/Å$^2$ on $\beta(2\times4)$ and $\beta2(2\times4)$, respectively. On both surfaces, the interface charge transfer is mainly localized above the As–As dimers, with negligible charge redistribution above the trench. Although the interface interactions are slightly smaller than Gr/GaAs(001)-(1 × 1), the potential fluctuations on these two Gr/GaAs reconstructed substrates are much larger. The uneven GaAs(001)-$\beta(2\times4)$ surface generates a high potential

above the As–As dimers (in the middle region along the $y$ direction) and a low potential above the trench, with a large fluctuation of 102.24 meV (Fig. S2 in the supplementary information). The distorted graphene also generates a sizeable potential fluctuation of 64.05 meV with a high potential in the middle region along the $x$ direction. Therefore, the potential sum Gr + GaAs is high near the center and low near the edge of the surface cell (red line in Fig. 2(d)), with a large fluctuation of 151.88 meV. Moreover, the interface charge transfer is relatively strong. The C atoms above the As–As dimers lose electrons about 0.002 $e$/atom–0.004 $e$/atom, while the As–As dimers gain electrons about 0.005 $e$/atom. The localized interface charge transfer significantly lowers the potentials above the As-As dimers, leading to the large difference between the blue and red lines near the center region, as shown in Fig. 2(d). The differences become minimal above the trench, where the interface charge transfer is negligible. As a result, the potential fluctuation of GaAs(001)-$\beta(2\times4)$ is 88.72 meV, much smaller than that of the potential sum Gr + GaAs. With one less As–As dimer, the isolated GaAs(001)-$\beta2(2\times4)$ surface generates smaller potential fluctuation, and the interface charge transfer is weaker. Therefore, the potential fluctuation on Gr/GaAs(001)-$\beta2(2\times4)$ is 83.63 meV, smaller than that on Gr/GaAs(001)-$\beta(2\times4)$.

From the above results, we can conclude that the uneven substrate, the distorted graphene monolayer, and the strong localized interface charge transfer all significantly contribute to the potential fluctuation. The graphene configuration and the interface charge transfer depend on the substrate structures. Therefore, changing the substrate reconstructions could change the graphene configuration as well as the interface charge transfer, and would significantly influence the potential fluctuation and the remote epitaxy effect.

### 3.3. Gr/GaN compound substrates

A GaN substrate with higher polarity has been reported to show a stronger remote epitaxy effect.[21] Here, we study the N-terminated $(000\bar{1})$, Ga-terminated (0001), and the nonpolar $(10\bar{1}0)$ surfaces covered by a graphene monolayer. Three reconstructions are considered for the $(000\bar{1})$ surface, as shown in Figs. 3(a) and 3(b). The interface with graphene on the $(000\bar{1})$ truncated surface is denoted as Gr/GaN$(000\bar{1})$-$(1\times1)$. The distance between graphene and the topmost N layer is 3.19 Å. The interface interaction is $-29.75$ meV/Å$^2$, larger than those of graphene on Si(001) and GaAs(001) truncated surfaces. This indicates that the interface interaction might depend on the polarity of the substrate.[21] One stable reconstruction of GaN$(000\bar{1})$ has an additional surface Ga adlayer,[49] and is denoted as GaN$(000\bar{1})$-$(1\times1)$-Ga here. The interface distance between graphene and the Ga adlayer is 3.62 Å, leading to a weak interface interaction of $-16.92$ meV/Å$^2$. Another stable reconstruction is GaN$(000\bar{1})$-$(3\times3)$, with one more Ga atom per $(3\times3)$ surface cell.[49,50] The distance between graphene and the Ga adlayer is 3.61 Å, similar to Gr/GaN$(000\bar{1})$-$(1\times1)$-Ga. However, the nearest distance from the topmost Ga atom to the C atoms is 2.65 Å, strengthening the interface interaction. As a result, the interface interaction is $-19.18$ meV/Å$^2$, slightly stronger than Gr/GaN$(000\bar{1})$-$(1\times1)$-Ga.

The difference charge densities in Fig. 3(b) indicate that electrons are mainly transferred from graphene to the GaN$(000\bar{1})$ surface, as determined by the polarity of the anion-terminated substrate. The charge transfer at the Gr/GaN$(000\bar{1})$-$(1\times1)$ interface is substantial due to the strong interface interaction. Both the first and second GaN bilayers gain electrons from graphene. The charge transfer is much weaker but still uniform at the Gr/GaN$(000\bar{1})$-$(1\times1)$-Ga interface. On the GaN$(000\bar{1})$-$(3\times3)$ surface, the interface charge transfer is slightly non-uniform. The Ga adlayer still obtains electrons from graphene, while the topmost Ga atom loses electrons to graphene.

The potential fluctuations on the three Gr/GaN$(000\bar{1})$ compound substrates are shown in Fig. 3(c). Although the interface interactions of Gr/GaN$(000\bar{1})$-$(1\times1)$ and Gr/GaN$(000\bar{1})$-$(1\times1)$-Ga are different, the potential fluctuations are calculated to be 25.96 meV and 28.05 meV, respectively, very similar to each other. Detailed calculations show that the flat GaN substrate and flat graphene of the two systems generate uniform potentials with similar fluctuations (Fig. S3 in the supplementary information), and the uniform interface charge transfer has little effect on the potential fluctuations. As a result, the potential fluctuations of the two compound substrates are close to each other, and very similar to their respective potential sum Gr + GaN (see the blue and red lines in Fig. 3(d)). In contrast, the potential distribution above Gr/GaN$(000\bar{1})$-$(3\times3)$ is non-uniform, with a large fluctuation of 93.31 meV. The potential of the isolated GaN$(0000\bar{1})$-$(3\times3)$ surface with a dip near the topmost Ga atom has a significant fluctuation of 90.70 meV and is the major contributor (Fig. 3(d) and Fig. S3 in the supplementary information). The isolated graphene monolayer generates a potential fluctuation of 19.84 meV. And the interface charge transfer only slightly influences the potential distribution above the topmost Ga atom.

The potential fluctuation also depends on the orientation of the substrate. We calculate the interface between graphene and the Ga-terminated GaN(0001) truncated surface. As shown in the right panel of Fig. 3(b), both the graphene monolayer and the surface Ga layer are distorted. A few C atoms shift down and bond to the surface Ga atoms with a bond length around 2.20 Å, resulting in a strong interface interaction. The average distance between graphene

and the surface Ga layer is 2.79 Å, and the interface interaction is −32.13 meV/Å$^2$, in good agreement with previous results of 2.78 Å and −28.6 meV/Å$^2$.[28,29] The isolated distorted graphene and GaN(0001) substrate generate non-uniform potentials with large fluctuations of 68.83 meV and 69.65 meV (Fig. S4 in the supplementary information), respectively. The potential sum Gr + GaN also has a large fluctuation of 120.98 meV, with low potentials near the center of the supercell (the red line in Fig. 3(d)). However, the strong interface interaction results in a significant and non-uniform charge transfer, which can significantly influence the potential distribution. As shown in Fig. 3(b), charge redistribution is mainly localized around the interface C–Ga bonds and the C atoms near the center of the supercell. Overall, graphene obtains 1.76 *e* from the GaN(0001) surface. This will induce a localized downward dipole near the center and increase the nearby potentials. As a result, the low potential near the center region is enhanced (between 3 Å–11 Å along the long diagonal in Fig. 3(c)), and thus the potential fluctuation of the Gr/GaN(0001) compound substrate is decreased to 72.42 meV. These results show that the inverse of the substrate polarity could change the magnitude of the potential fluctuation through graphene. The substrate orientation is one of the key factors for remote epitaxy.

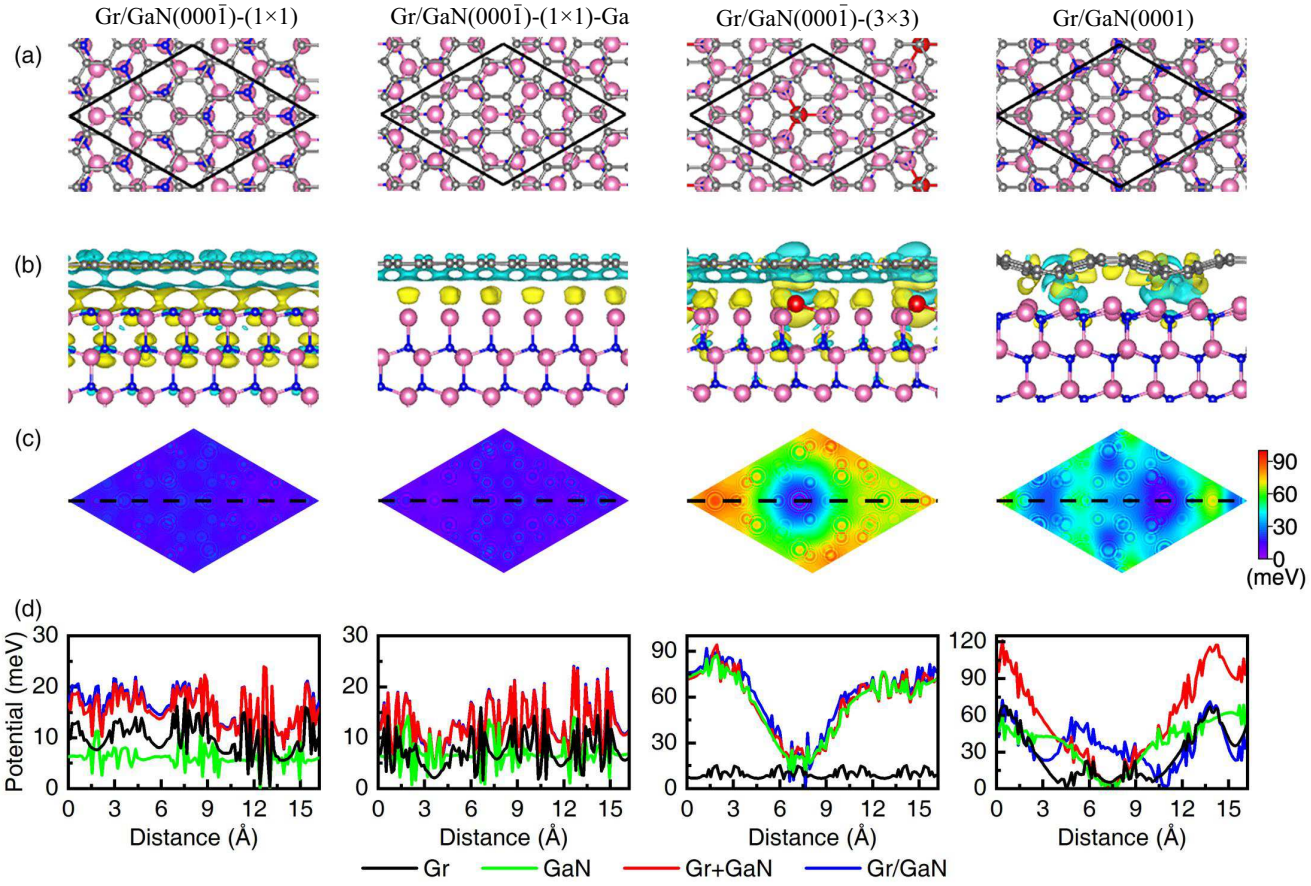



**Fig. 3.** (a) Top views of the Gr/GaN(000$\bar{1}$)-(1 × 1), Gr/GaN(000$\bar{1}$)-(1 × 1)-Ga, Gr/GaN(000$\bar{1}$)-(3 × 3), and Gr/GaN(0001) interfaces. The pink, blue, and gray balls represent Ga, N, and C atoms, respectively. The red balls in GaN(000$\bar{1}$)-(3 × 3) represent the topmost surface Ga atoms. (b) Difference charge densities of the four interfaces. The isosurface value is 0.0002 *e*/Bohr$^3$ in Gr/GaN(000$\bar{1}$) interfaces and 0.002 *e*/Bohr$^3$ in Gr/GaN(0001). (c) Potential fluctuation maps of the four interfaces. (d) Potential fluctuations of the isolated graphene Gr, isolated substrate GaN, potential sum Gr + GaN, and compound substrate Gr/GaN along the black dashed lines in panel (c).

We next study the remote epitaxy of the non-polar GaN(10$\bar{1}$0) surface covered by graphene. As shown in Figs. 4(a) and 4(b), graphene is flat on the surface with an interlayer distance of 3.19 Å, leading to a weak vdW interface interaction of −19.56 meV/Å$^2$. We analyze the contributions to the potential fluctuation in Gr/GaN(10$\bar{1}$0). The potential fluctuations of the isolated flat graphene and the substrate are 19.00 meV and 31.55 meV, respectively. The fluctuation of the potential sum Gr + GaN is 40.61 meV (Fig. S5 in the supplementary information), very close to the fluctuation of 41.71 meV of the Gr/GaN(10$\bar{1}$0) compound substrate (Fig. 4(c)). Moreover, the potential distribution of the compound substrate follows a similar pattern to the isolated substrate, which is high above the surface N and low above the surface Ga, as seen in Fig. 4(d). This indicates that the major contributor to the potential fluctuation is the non-polar substrate, whereas the interface charge transfer makes a minor contribution. Due to the different electron negativities

of Ga and N atoms, the C atoms above Ga atoms gain electrons, while those above N atoms lose electrons, as shown in Fig. 4(b). This bidirectional charge transfer has also been reported in a Gr/ZnO$(11\bar{2}0)$ interface.[27] The $z$-component of the resulting interface dipole is only 0.01 Debye/Å$^2$, much smaller than the other systems. Therefore, the interface charge transfer has a small effect on the potential fluctuation. In this case, we can see that the potential fluctuation from the non-polar substrate could be large enough for remote epitaxy. In a previous study, Jeong *et al.* grew ZnO$[11\bar{2}0]$ nanorods on a graphene covered ZnO$(11\bar{2}0)$ substrate, where the ZnO nanorods had the same lattice arrangements as the nonpolar substrate.[27] Therefore, it is possible to change the orientation of the overlayer in remote epitaxy by changing the orientation of the underlying semiconductor substrates.

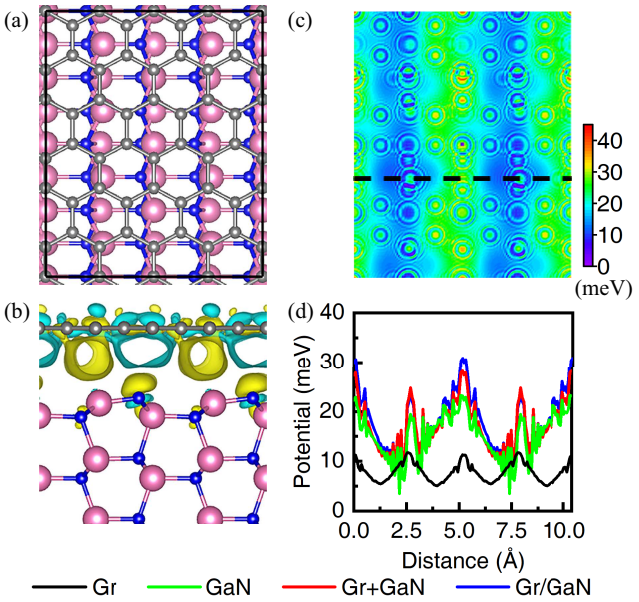



**Fig. 4.** (a) Top view of the Gr/GaN$(10\bar{1}0)$ interface. (b) Difference charge densities of the Gr/GaN$(10\bar{1}0)$ interface. Isosurface value is 0.0002 $e$/Bohr$^3$. (c) Potential fluctuation map of the Gr/GaN$(10\bar{1}0)$ interface. (d) Potential fluctuations of the isolated graphene Gr, isolated substrate GaN, potential sum Gr + GaN, and compound substrate Gr/GaN along the black dashed line in panel (c).

## 4. Adsorption of adatoms

It is believed that the potential from the semiconductor substrate can penetrate the graphene monolayer and influence the adsorption of the coming adatoms, which is essential for the nucleation and initial growth of the overlayer.[21,51] To study the influence of the underlying substrate on the adsorption of adatoms, we compare the adsorption of Ga, As, and N adatoms on isolated graphene and Gr/sub compound substrates. The adsorption energy $E_{\rm ad}$ of an adatom is defined as

$$E_{\rm ad} = E_{\rm tot} - E_{\rm atom} - E_{\rm sub}, \tag{3}$$

where $E_{\rm tot}$, $E_{\rm atom}$, and $E_{\rm sub}$ are the energies of the adsorption system, the isolated adatom, and the isolated substrate (graphene or Gr/sub), respectively. On the isolated graphene monolayer, there are three stable adsorption sites for adatoms: the hollow (H) site above the center of the hexagon, the bridge (B) site above the center of a C–C bond, and the top (T) site above a C atom. As shown in Table 1, the adsorption energies of the Ga adatom on the three sites are pretty similar.[52] At the most stable H site, the C–Ga bond length is 2.71 Å, and the adsorption energy is −1.01 eV. We further show the difference charge density in Fig. 5(a). The difference charge density $\Delta\rho$ is defined as

$$\Delta\rho = \rho_{\rm tot} - \rho_{\rm atom} - \rho_{\rm sub}, \tag{4}$$

where $\rho_{\rm tot}$, $\rho_{\rm atom}$, and $\rho_{\rm sub}$ are the charge densities of the adatom/sub adsorption system, the isolated adatom, and the isolated substrate, respectively. As seen in Fig. 5(a), the Ga adatom loses 0.61 $e$ to graphene and is polarized. On the other hand, the N adatom prefers to adsorb at the B site. The adsorption energy is −0.93 eV, and the N–C bond length is 1.47 Å, in good agreement with previous calculations of −0.92 eV and 1.45 Å, respectively.[53] As shown in Fig. 5(e), the nonmetallic N adatom gains 0.55 $e$ from graphene and locally distorts the graphene structure. The adsorption energies of the N adatom on the other two sites are much weaker. The adsorption energies of the As adatom on the three sites are around −0.2 eV, indicating that it is difficult for the As atom to adsorb on graphene.

**Table 1.** The adsorption energy $E_{\rm ad}$, adatom–C bond length $l$, and charge transfer amount $\Delta n$ of Ga, N, and As adatoms adsorbed on the graphene monolayer. The positive and negative signs of $\Delta n$ correspond to electron accumulation and depletion on adatoms, respectively.

| adatom | Site | $E_{\rm ad}$ (eV) | $l$ (Å) | $\Delta n$ ($e$) |
|---|---|---|---|---|
| Ga | H | −1.01 | 2.71 | −0.61 |
| | B | −0.93 | 2.48 | −0.58 |
| | T | −0.93 | 2.39 | −0.56 |
| N | H | −0.10 | 3.25 | +0.30 |
| | B | −0.93 | 1.47 | +0.55 |
| | T | -0.08 | 1.47 | +0.39 |
| As | H | −0.16 | 3.76 | −0.01 |
| | B | −0.15 | 3.58 | −0.01 |
| | T | −0.15 | 3.52 | −0.01 |

We find that the underlying semiconductor can strongly influence the adsorption sites and adsorption energies of adatoms on Gr/sub compound substrates. On Gr/GaN$(000\bar{1})$-$(1\times1)$, the electron transfer direction from Ga to graphene is the same as that from graphene to the GaN substrate, as shown in Fig. 5(b). This results in two interface dipoles along the same direction, increasing the adsorption of the Ga adatom on Gr/GaN$(000\bar{1})$-$(1\times1)$. The most stable adsorption site of the Ga adatom is still the H site, with adsorption energy around −1.56 eV. The adsorption on the B site is slightly less favorable, with a lower adsorption energy of −1.47 eV. But the T

site becomes unfavorable for the Ga adatom. Note that the stable adsorption sites on the Gr/GaN compound substrate are slightly shifted away from the high symmetry sites due to the influence of the underlying GaN substrate. The adsorption energies on different adsorption sites are similar, consistent with the small potential fluctuation above Gr/GaN$(000\bar{1})$-$(1\times1)$. The N adatom also prefers to adsorb on B sites, as on the isolated graphene. As shown in Fig. 5(f), graphene under the N adatom is locally distorted, facilitating the $sp^3$ hybridization between N and C atoms. The N–C bond length is 1.46 Å, slightly shorter than that on isolated graphene. Therefore, the N adsorption energy is slightly enhanced to around −1.08 eV. The higher adsorption energy of Ga than N adatom indicates that it is easier for Ga adatoms to adsorb and nucleate on Gr/GaN$(000\bar{1})$-$(1\times1)$. This will probably lead to the initial growth of a N-polar overlayer, as on the isolated graphene.

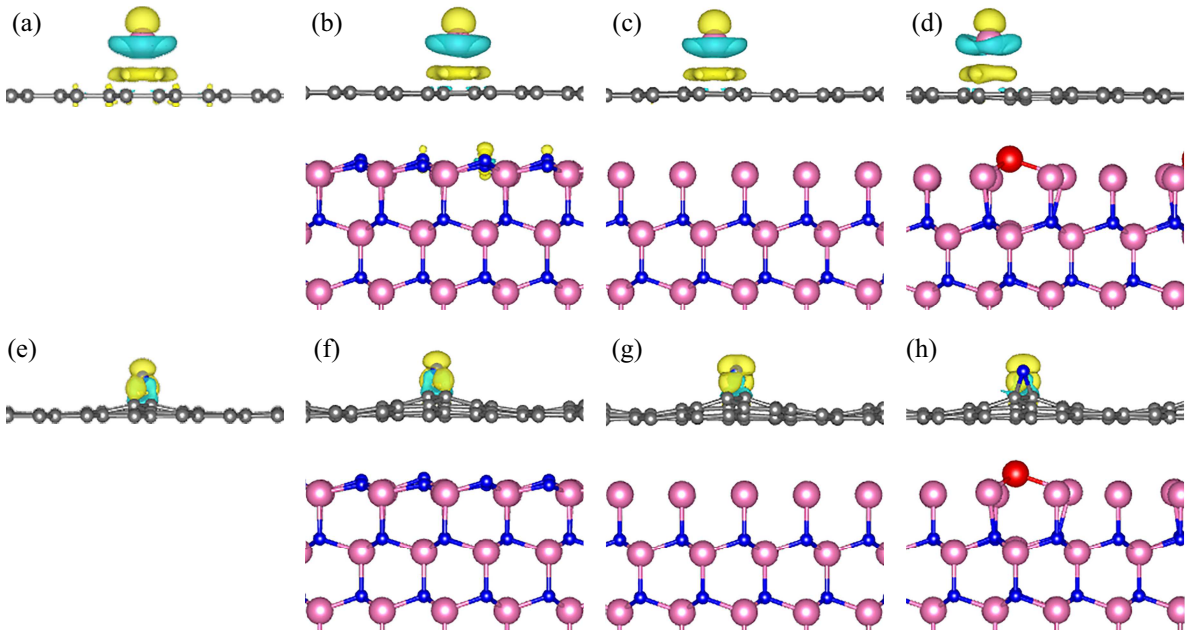



**Fig. 5.** Difference charge densities of one Ga adatom on (a) isolated graphene, (b) Gr/GaN$(000\bar{1})$-$(1\times1)$, (c) Gr/GaN$(000\bar{1})$-$(1\times1)$-Ga, and (d) Gr/GaN$(000\bar{1})$-$(3\times3)$ substrates. Difference charge densities of one N adatom on (e) isolated graphene, (f) Gr/GaN$(000\bar{1})$-$(1\times1)$, (g) Gr/GaN$(000\bar{1})$-$(1\times1)$-Ga, and (h) Gr/GaN$(000\bar{1})$-$(3\times3)$ substrates. The isosurface values are 0.003 $e$/Bohr$^3$ and 0.1 $e$/Bohr$^3$ for Ga and N adsorption, respectively.

The interface charge transfer can further influence the adsorption of Ga and N adatoms. On Gr/GaN$(000\bar{1})$-$(1\times1)$-Ga, Ga and N adatoms prefer to adsorb on H and B sites, respectively, as shown in Figs. 5(c) and 5(g). Compared to Gr/GaN$(000\bar{1})$-$(1\times1)$, the surface Ga layer weakens the electron transfer from graphene to the GaN surface. This is unfavorable for the electron transfer from the Ga adatom to graphene but beneficial for the electron transfer from graphene to the N adatom. Therefore, the adsorption energy of the Ga adatom at the H site is decreased to around −1.19 eV. The adsorption of the N adatom on B sites becomes stronger, with shorter N–C bond lengths around 1.44 Å and larger adsorption energies about −1.14 eV.

On Gr/GaN$(000\bar{1})$-$(3\times3)$, the topmost Ga atom on the GaN surface can transfer electrons to graphene, as discussed in Subsection 3.3. This will further facilitate N adsorption by enhancing the electron transfer from graphene to N, but is quite unfavorable for Ga adsorption. As a result, the adsorption of the N adatom is enhanced to around −1.2 eV, and that of the Ga adatom is decreased to around −0.90 eV. Due to the reversed charge transfer around the topmost surface Ga atom, the N adsorption energy exceeds Ga on Gr/GaN$(000\bar{1})$-$(3\times3)$. We also find that the adsorption energies of both Ga and N adatoms depend on the interface structures. For Ga adatom, the adsorption above the topmost Ga (−0.91 eV in Fig. 5(d)) is stronger than that far away from the topmost Ga (−0.88 eV, not shown), due to a shorter distance between the adatom and the underlying GaN substrate near the topmost Ga atom. However, the adsorption energies of N adatoms near the topmost Ga atom (−1.18 eV) are slightly weaker than the other positions (around −1.20 eV). This can be understood by the local structure distortion around the N adatom. As shown in Fig. 5(h), the two C atoms under the N adatom are lifted by 0.92 Å, increasing the distance to the topmost Ga atom up to 3.41 Å. This will decrease the interaction between the graphene and the GaN substrate and lower the total energy of the adsorption system.

The dependence on substrate morphology of the adsorption energy is general in other substrates. For example, on Gr/GaAs(001)-$\beta(2\times4)$, both Ga and As adatoms above the As–As dimers have stronger adsorption energies than above the trench, due to the shorter distance between the adatom

and the underlying substrate. The adsorption energies of the Ga adatom above the As–As dimer and above the trench are −1.24 eV and −1.18 eV, respectively. For the As adatom, the adsorption energies are −0.25 eV and −0.23 eV, respectively.

We also find that the adsorption of adatoms can be influenced by the orientation of the substrates. On Gr/GaN(0001), the adsorption energies of the Ga adatoms on different sites (near H sites) are between −1.09 eV and −1.36 eV, while those for the N adatoms (near B sites) are between −2.19 eV and −2.38 eV (Fig. S6 in the supplementary information). Both adatoms have larger adsorption energies near the curved region of the graphene due to the stronger $sp^3$ hybridization. Overall, the Ga adsorption energies are consistently smaller than the N adsorption energies by about 1 eV. The reversed order of the adsorption energies of Ga and N adatoms can be attributed to the interface charge transfer. As discussed in Subsection 3.3, the Ga-terminated (0001) surface loses electrons to graphene, facilitating electron transfer from graphene to the N adatom. Therefore, the adsorption of the N adatom is significantly enhanced and even stronger than the adsorption of the Ga adatom. This indicates that N atoms can easily adsorb and nucleate on the Gr/GaN(0001) compound substrate, leading to the growth of a Ga-polar overlayer. Therefore, it is possible to change the adsorption strength of the coming adatoms or even change the polarity of the overlayers by reversing the polarity of the substrate during remote epitaxy.

On the Gr/GaN$(10\bar{1}0)$ compound substrate, the adsorption energies of Ga and N adatoms are determined by the surface atomic arrangements and orientation of the underlying substrate. The Ga adsorption energies are between −1.38 eV and −1.42 eV, and the N adsorption energies are between −1.26 eV and −1.39 eV (Fig. S7 in the supplementary information). For both adatoms, the adsorption energies above the surface N are always slightly larger than that above the surface Ga, since the surface N atoms are higher than the surface Ga atoms by 0.22 Å. On this compound substrate, both Ga and N adatoms have relatively strong and similar adsorption energies. Therefore, it is possible that both adatoms can adsorb and nucleate on Gr/GaN$(10\bar{1}0)$, leading to the growth of a non-polar overlayer. Previous experiments have reported the growth of non-polar ZnO$[11\bar{2}0]$ nanorods on Gr/ZnO$(11\bar{2}0)$.[27] This is strong evidence that the orientation of the overlayer can be controlled by the substrate orientation in remote epitaxy.

From the above results, we can conclude that the adsorption of adatoms on a Gr/sub compound substrate highly depends on the interface morphology, substrate orientation, and the interface charge transfer, but shows little correlation to the potential fluctuation. The potential fluctuation with less than 100 meV in magnitude cannot sufficiently explain the changes in adsorption energies of both Ga and N atoms on different Gr/sub compound substrates. Nevertheless, the potential fluctuation could be more relevant to the long-range arrangement of adatoms on compound substrates, which is also essential for the nucleation and growth of the epilayer.

## 5. Conclusion

Using first-principles calculations, we systematically study the potential fluctuations and adatom adsorption energies on graphene covered Si, GaAs, and GaN substrates to understand the remote epitaxy mechanism. We analyze the interface interactions and the contributions to the potential fluctuations of different Gr/sub compound substrates. We find that the potential fluctuation highly depends on the Gr/sub interface structure and the interface charge transfer. The uneven semiconductor surface and graphene monolayer could generate non-uniform potential distributions with large fluctuations. In addition, the non-uniform interface charge transfer will locally modify the potential distribution and further contribute to the fluctuation. The adsorption energies of adatoms on the Gr/sub are highly correlated to the semiconductor reconstructions, orientations, and interface charge transfer. Changing the semiconductor reconstruction and orientation can change the interface charge transfer and the magnitude of adsorption energy, and even reverse the order of cation and anion adsorption energies. Our calculations indicate that semiconductor reconstruction and orientation are essential for the nucleation and the orientation of the overlayer. It is possible to control the overlayer growth by changing the underlying semiconductor substrate in remote epitaxy.

## Acknowledgments

The calculations were performed on the TH-1A supercomputer at the National Supercomputing Center in Tianjin, China. Project supported by the National Key R&D Program of China (Grant No. 2019YFA0708202) and the National Natural Science Foundation of China (Grant No. 12074369).

## References

[1] Chung K, Lee C H and Yi G C 2010 *Science* **330** 655
[2] Hong Y J, Lee C H, Yoon A, Kim M, Seong H K, Chung H J, Sone C, Park Y J and Yi G C 2011 *Adv. Mater.* **23** 3284
[3] Yang J, Yan D and Jones T S 2015 *Chem. Rev.* **115** 5570
[4] Wang C H, Cheng K Y, Yang S J and Hwang F C 1985 *J. Appl. Phys.* **58** 757
[5] Vispute R D, Talyansky V, Choopun S, Sharma R P, Venkatesan T, He M, Tang X, Halpern J B, Spencer M G, Li Y X, Salamanca-Riba L G, Iliadis A A and Jones K A 1998 *Appl. Phys. Lett.* **73** 348
[6] Currie M T, Samavedam S B, Langdo T A, Leitz C W and Fitzgerald E A 1998 *Appl. Phys. Lett.* **72** 1718
[7] Luan H C, Lim D R, Lee K K, Chen K M, Sandland J G, Wada K and Kimerling L C 1999 *Appl. Phys. Lett.* **75** 2909
[8] Andre C L, Wilt D M, Pitera A J, Lee M L, Fitzgerald E A and Ringel S A 2005 *J. Appl. Phys.* **98** 014502
[9] Daruka I and Barabási A L 1997 *Phys. Rev. Lett.* **79** 3708

[10] Massies J and Grandjean N 1993 *Phys. Rev. Lett.* **71** 1411
[11] Song T L, Chua S J, Fitzgerald E A, Chen P and Tripathy S 2003 *Appl. Phys. Lett.* **83** 1545
[12] Camarero J, Ferrón J, Cros V, Gómez L, Vázquez de Parga A L, Gallego J M, Prieto J E, de Miguel J J and Miranda R 1998 *Phys. Rev. Lett.* **81** 850
[13] Utama M I B, Zhang Q, Zhang J, Yuan Y, Belarre F J, Arbiol J and Xiong Q 2013 *Nanoscale* **5** 3570
[14] Alaskar Y, Arafin S, Wickramaratne D, Zurbuchen M A, He L, McKay J, Lin Q, Goorsky M S, Lake R K and Wang K L 2014 *Adv. Funct. Mater.* **24** 6629
[15] Kim J, Bayram C, Park H, Cheng C W, Dimitrakopoulos C, Ott J A, Reuter K B, Bedell S W and Sadana D K 2014 *Nat. Commun.* **5** 4836
[16] Dang W, Peng H, Li H, Wang P and Liu Z 2010 *Nano Lett.* **10** 2870
[17] Liu Y, Weinert M and Li L 2012 *Phys. Rev. Lett.* **108** 115501
[18] Gehring P, Gao B F, Burghard M and Kern K 2012 *Nano Lett.* **12** 5137
[19] Munshi A M, Dheeraj D L, Fauske V T, Kim D C, van Helvoort A T J, Fimland B O and Weman H 2012 *Nano Lett.* **12** 4570
[20] Kim Y, Cruz S S, Lee K, Alawode B O, Choi C, Song Y, Johnson J M, Heidelberger C, Kong W, Choi S, Qiao K, Almansouri I, Fitzgerald E A, Kong J, Kolpak A M, Hwang J and Kim J 2017 *Nature* **544** 340
[21] Kong W, Li H, Qiao K, *et al.* 2018 *Nat. Mater.* **17** 999
[22] Badokas K, Kadys A, Mickevičius J, Ignatjev I, Skapas M, Stanionytė S, Radiunas E, Juška G and Malinauskas T 2021 *J. Phys. D* **54** 205103
[23] Jeong J, Wang Q, Cha J, Jin D K, Shin D H, Kwon S, Kang B K, Jang J H, Yang W S, Choi Y S, Yoo J, Kim J K, Lee C H, Lee S, Zakhidov A A, Hong S, Kim M J and Hong Y J 2020 *Sci. Adv.* **6** eaaz5180
[24] Journot T, Okuno H, Mollard N, Michon A, Dagher R, Gergaud P, Dijon J, Kolobov A V and Hyot B 2019 *Nanotechnology* **30** 505603
[25] Chang H, Chen Z, Li W, Yan J, Hou R, Yang S, Liu Z, Yuan G, Wang J, Li J, Gao P and Wei T 2019 *Appl. Phys. Lett.* **114** 091107
[26] Chen Z, Liu Z, Wei T, Yang S, Dou Z, Wang Y, Ci H, Chang H, Qi Y, Yan J, Wang J, Zhang Y, Gao P, Li J and Liu Z 2019 *Adv. Mater.* **31** 1807345
[27] Jeong J, Min K A, Shin D H, Yang W S, Yoo J, Lee S W, Hong S and Hong Y J 2018 *Nanoscale* **10** 22970
[28] Jeong J, Min K A, Kang B K, Shin D H, Yoo J, Yang W S, Lee S W, Hong S and Hong Y J 2018 *Appl. Phys. Lett.* **113** 233103
[29] Jeong J, Jin D K, Cha J, Kang B K, Wang Q, Choi J, Lee S W, Mikhailovskii V Y, Neplokh V, Amador-Mendez N, Tchernycheva M, Yang W S, Yoo J, Kim M J, Hong S and Hong Y J 2020 *ACS Appl. Nano Mater.* **3** 8920
[30] Jiang J, Sun X, Chen X, *et al.* 2019 *Nat. Commun.* **10** 4145
[31] Wang D, Lu Y, Meng J, Zhang X, Yin Z, Gao M, Wang Y, Cheng L, You J and Zhang J 2019 *Nanoscale* **11** 9310
[32] Jia R, Kum H S, Sun X, Guo Y, Wang B, Fang P, Jiang J, Gall D, Lu T M, Washington M, Kim J and Shi J 2021 *J. Vac. Sci. Technol. A* **39** 040405
[33] Guo Y, Sun X, Jiang J, Wang B, Chen X, Yin X, Qi W, Gao L, Zhang L, Lu Z, Jia R, Pendse S, Hu Y, Chen Z, Wertz E, Gall D, Feng J, Lu T M and Shi J 2020 *Nano Lett.* **20** 33
[34] Yoo D, Lee K, Tchoe Y, Guha P, Ali A, Saroj R K, Lee S, Islam A B M H, Kim M and Yi G C 2021 *Sci. Rep.* **11** 17524
[35] Lee C H, Kim Y J, Hong Y J, Jeon S R, Bae S, Hong B H and Yi G C 2011 *Adv. Mater.* **23** 4614
[36] Kresse G and Furthmuller J 1996 *Phys. Rev. B* **54** 11169
[37] Blöchl P E 1994 *Phys. Rev. B* **50** 17953
[38] Perdew J P, Burke K and Ernzerhof M 1996 *Phys. Rev. Lett.* **77** 3865
[39] Monkhorst H J and Pack J D 1976 *Phys. Rev. B* **13** 5188
[40] Grimme S, Antony J, Ehrlich S and Krieg H 2010 *J. Chem. Phys.* **132** 154104
[41] Niu M, Li D, Sheng B, Shao X, Liu W and Wang Z 2011 2011 *IEEE International Conference on Mechatronics and Automation*, August 7–10, 2011 Beijing, China, p. 1423
[42] Kim Y S, Marsman M, Kresse G, Tran F and Blaha P 2010 *Phys. Rev. B* **82** 205212
[43] Zhang Z, Qian Q, Li B and Chen K J 2018 *ACS Appl. Mater. Interfaces* **10** 17419
[44] Leszczynski M, Teisseyre H, Suski T, Grzegory I, Bockowski M, Jun J, Porowski S, Pakula K, Baranowski J M, Foxon C T and Cheng T S 1996 *Appl. Phys. Lett.* **69** 73
[45] Pavlova T V, Zhidomirov G M and Eltsov K N 2018 *J. Phys. Chem. C* **122** 1741
[46] Henkelman G, Arnaldsson A and Jónsson H 2006 *Comput. Mater. Sci.* **36** 354
[47] Ohtake A 2008 *Surf. Sci. Rep.* **63** 295
[48] Schmidt W G and Bechstedt F 1996 *Surf. Sci.* **360** L473
[49] Smith A R, Feenstra R M, Greve D W, Neugebauer J and Northrup J E 1997 *Phys. Rev. Lett.* **79** 3934
[50] Smith A R, Feenstra R M, Greve D W, Shin M S, Skowronski M, Neugebauer J and Northrup J E 1998 *J. Vac. Sci. Technol. B* **16** 2242
[51] Pashley D W 1999 *Mater. Sci. Technol.* **15** 2
[52] Chan K T, Neaton J B and Cohen M L 2008 *Phys. Rev. B* **77** 235430
[53] Rani B and Dharamvir K 2014 *Int J Quantum Chem* **114** 1619